


RESEARCH

Open Access



# Inhibition of acid sphingomyelinase reduces reactive astrocyte secretion of mitotoxic extracellular vesicles and improves Alzheimer's disease pathology in the 5xFAD mouse

Simone M. Crivelli<sup>1</sup>, Zainuddin Quadri<sup>1</sup>, Hemendra J. Vekaria<sup>2,3,4</sup>, Zhihui Zhu<sup>1</sup>, Priyanka Tripathi<sup>1</sup>, Ahmed Elsherbini<sup>1</sup>, Liping Zhang<sup>1</sup>, Patrick G. Sullivan<sup>2,3,4</sup> and Erhard Bieberich<sup>1,4\*</sup> 

## Abstract

In Alzheimer's disease (AD), reactive astrocytes produce extracellular vesicles (EVs) that affect mitochondria in neurons. Here, we show that A $\beta$ -induced generation of the sphingolipid ceramide by acid sphingomyelinase (A-SMase) triggered proinflammatory cytokine (C1q, TNF- $\alpha$ , IL-1 $\alpha$ ) release by microglia, which induced the reactive astrocytes phenotype and secretion of EVs enriched with ceramide. These EVs impeded the capacity of neurons to respond to energy demand. Inhibition of A-SMase with Arc39 and Imipramine reduced the secretion of cytokines from microglia, prompting us to test the effect of Imipramine on EV secretion and AD pathology in the 5xFAD mouse model. Brain derived-EVs from 5xFAD mice treated with Imipramine contained reduced levels of the astrocytic marker GFAP, ceramide, and A $\beta$  and did not impair mitochondrial respiration when compared to EVs derived from untreated 5xFAD brain. Consistently, Imipramine-treated 5xFAD mice showed reduced AD pathology. Our study identifies A-SMase inhibitors as potential AD therapy by preventing cytokine-elicited secretion of mitotoxic EVs from astrocytes.

**Keywords** Imipramine, Extracellular vesicle, Acid sphingomyelinase, Mitochondria, 5xFAD, Microglia, Astrocytes, TNF- $\alpha$ , IL-1 $\alpha$ , C1q

## Introduction

Current treatments for Alzheimer's disease (AD) mainly provide symptomatic, short-term benefits, without affecting the cause and progression of the disease. Therefore, a major challenge in the AD research field is

to develop new therapies that target causative factors of AD for the prevention or delay of disease onset. Several lines of evidence link the sphingolipid ceramide (Cer) to AD pathophysiology. Firstly, global levels of specific Cer species are elevated in AD patients compared to healthy controls [1–4]. Secondly, high levels of long chain Cer (C22 or C24) in plasma are associated with an increased risk to develop mild cognitive impairment or AD [5, 6]. Thirdly, cerebral spinal fluid detection of Cer levels correlates with some forms of amyloid- $\beta$  (A $\beta$ ) in individuals at high risk of developing AD, implying early involvement of Cer in the pathogenesis of the disease [7]. Lastly, in agreement with these observations, enzymes responsible for Cer anabolic or catabolic production are abnormally transcribed or activated in AD

\*Correspondence:

Erhard Bieberich  
erhard.bieberich@uky.edu

<sup>1</sup> Department of Physiology, University of Kentucky College of Medicine, 780 Rose Street MS519, Lexington, KY 40536, USA

<sup>2</sup> Department of Neuroscience, University of Kentucky, Lexington, KY 40536, USA

<sup>3</sup> Spinal Cord and Brain Injury Research Center (SCoBIRC), University of Kentucky, Lexington, KY, USA

<sup>4</sup> Veterans Affairs Medical Center, Lexington, KY 40502, USA



© The Author(s) 2023. **Open Access** This article is licensed under a Creative Commons Attribution 4.0 International License, which permits use, sharing, adaptation, distribution and reproduction in any medium or format, as long as you give appropriate credit to the original author(s) and the source, provide a link to the Creative Commons licence, and indicate if changes were made. The images or other third party material in this article are included in the article's Creative Commons licence, unless indicated otherwise in a credit line to the material. If material is not included in the article's Creative Commons licence and your intended use is not permitted by statutory regulation or exceeds the permitted use, you will need to obtain permission directly from the copyright holder. To view a copy of this licence, visit <http://creativecommons.org/licenses/by/4.0/>. The Creative Commons Public Domain Dedication waiver (<http://creativecommons.org/publicdomain/zero/1.0/>) applies to the data made available in this article, unless otherwise stated in a credit line to the data.

brain tissue compared to healthy controls [8, 9]. What remains to be clarified is whether these observations are a causative or a consequent event in the pathophysiology of AD and the druggability of Cer metabolism to prevent AD [10].

One of the key enzymes generating Cer and linked to AD is acid sphingomyelinase (A-SMase), which is a phosphodiesterase that breaks down sphingomyelin to form Cer in the lysosomes and at the plasma membrane of cells. In the brains of AD patients, the expression levels of A-SMase are increased and the enzymatic activity abnormally high [9, 11]. A-SMase is activated by oxidative stress [12] or TNF- $\alpha$  [13], which are produced in response to A $\beta$  peptides by brain-resident cells, such as microglia, in AD [14]. Microglia are the first responders to A $\beta$  peptide oligomers in the brain, by secreting proinflammatory factors including TNF- $\alpha$ , IL-1 $\alpha$  and Complement factor C1q, all of which activate astrocytes [15]. In the context of AD, reactive astrocytes fail to provide structural and metabolic support to neurons and produce extracellular vesicles (EVs) enriched in Cer that are taken-up by neurons [16, 17]. Co-transport of elevated Cer with A $\beta$  peptide as cargo in these vesicles seems to have a mitotoxic effect [16, 17]. Therefore, the SM-Cer pathway controlled by A-SMase may be a potential target in AD by reducing secretion of proinflammatory factors [18], thereafter preventing formation of astrocyte-derived mitotoxic EVs. Classic tricyclic anti-depressants (TCAs) such as Imipramine inhibit the activity of A-SMase [19, 20] by displacing the enzyme from its membrane-bound substrate [21]. This causes the lysosomal enzyme to be degraded at a faster rate [22]. Due to this peculiar mechanism, these pharmacological agents have been defined as functional inhibitors of A-SMase (FIASMA) [23].

In this study, we hypothesized that Cer generated by A-SMase sustains the inflammatory response by controlling the release of TNF- $\alpha$ , IL-1 $\alpha$  and C1q from microglia, and subsequently activation of astrocytes to produce of EVs that induce mitochondria-dependent apoptosis in neurons. We found that inhibition of A-SMase in microglia isolated from adult 5xFAD mice reduced A $\beta$ -induced release of TNF- $\alpha$ , IL-1 $\alpha$  and C1q, proinflammatory cytokines that induced secretion of mitotoxic EVs from reactive astrocytes. Administration of Imipramine to 5xFAD mice reduced proinflammatory microglia, reactive astrocytes, and neuronal death. Brain derived-EVs of 5xFAD mice treated with Imipramine were less neurotoxic compared to EVs derived from 5xFAD brain treated with vehicle. Our study highlights A-SMase as a target in AD and warrants synthesis of brain permeable specific A-SMase inhibitors as anti-AD therapeutic strategies.

## Material and methods

### Animals

C57BL/6 wild type (WT) and 5xFAD mice were bred in-house. Animals were socially housed under a 12 h light/dark cycle in individually ventilated cages. Food and water were provided ad libitum throughout the study. Imipramine (Sigma-Aldrich, I7379) was dissolved in Dulbecco's Phosphate-Buffered Saline (DPBS) without calcium and magnesium (Corning, 21-031-CV) and administered intraperitoneally (IP) at the dose 15  $\mu$ g/g animals given every 24 h. The volume injected per animal was adjusted to 0.2 mL and administered with insulin syringes. The vehicle DPBS was used as a control. Treatment was given for 28 days starting at the age of 2 months to a total of 36 animals equally distributed between vehicle and Imipramine. Experimental groups were divided based on genotype (WT vehicle N=9, WT Imipramine N=9, 5xFAD vehicle N=9, and 5xFAD Imipramine N=9) and balanced for sex. At the end of the experiment, mice were euthanized. Prior to intracardial perfusion with ice-cold PBS, blood was withdrawn. Next, the brain was quickly removed, and one half was dissected into fore-brain and hippocampus and used for extracellular vesicle (EV) isolation, western blotting, and lipid analysis. The other half was immersed in 4% paraformaldehyde (PFA) solution (Thermo Scientific, J19943-K2) for cryo-sectioning and fluorescence labelling. All experiments using mice to generate primary cell cultures or drug testing were carried out according to the Animal Use Protocol approved by the Institutional Animal Care and Use Committee at the University of Kentucky.

### Preparation of primary microglia and astrocytes

**Microglia.** Primary microglia were isolated and cultivated from adult WT at 4 weeks of age using MACS<sup>®</sup> Tissue Dissociation Kit (130-107-677) from Miltenyi Biotec in 12 well plates. Microglia were cultured in DMEM (Corning, 10-013-CV) containing 10% FBS (Atlanta biologicals, S11550) till the day of the experiment when cells were deprived of serum for 24 h. A $\beta_{1-42}$  peptide (AnaSpec, AS-20276) was incubated at 4 °C overnight to allow oligomer formation in serum free media. The next day, 2  $\mu$ M were added to microglia in presence or absence of 5  $\mu$ M ARC39 (1-Aminodecylidene bis-Phosphonic Acid, Cayman Chemical, 13,583) or 10  $\mu$ M of Imipramine. Scrambled A $\beta_{1-42}$  (Anaspec, AS-25382) was used as a control.

**Astrocytes.** Primary astrocytes were isolated and cultivated from adult WT brains at 4 weeks of age using Miltenyi Biotec MACS<sup>®</sup> Tissue Dissociation Kit (130-107-677) in 12 well plates. Astrocytes were cultured in DMEM (Corning, 10-013-CV) containing 10% FBS (Atlanta biologicals, S11550) till the day of the

experiment when cells were deprived of serum for 24 h. 0.5 mL of the microglia conditioned medium was used to incubate astrocytes for 24 h. To characterize EV release in presence of proinflammatory factors, astrocytes were isolated from post-natal mice at day 3 as previously described in T75 flasks [24]. Astrocytes were stimulated with 400 ng/mL of C1q (Abcam, ab282858), 30 ng/mL of TNF- $\alpha$  (Abcam, ab259411) and 3 ng/mL of IL-1 $\alpha$  (Milipore Sigma, I3901-5UG).

#### Cytokine analysis and A-SMase activity assay

After 18 h treatment with 5  $\mu$ M of ARC39 or 10  $\mu$ M of Imipramine, conditioned media from primary microglia were collected and used for detection of secreted cytokines TNF $\alpha$ , IL-1 $\alpha$ , (Biolegend, 430904 and 433404) and C1q (Abcam, ab291069) by ELISA following the manufacturers' instructions.

A-SMase activity was determined in microglia cellular lysate using an A-SMase assay kit (Echelon Biosciences, K-3200) following the company's instructions. After incubation with or without A $\beta$ <sub>1-42</sub> peptide (rPeptide, A-1163-2) in the presence of 10  $\mu$ M of Imipramine (Sigma-Aldrich, I7379) or 10 ng/mL of TNF- $\alpha$  receptor inhibitor (MedChemExpress, HY-P9970) or 10  $\mu$ M of TLR4 Inhibitor (TAK-242), microglia were sonicated in ice-cold lysis buffer containing 150 mM NaCl, 50 mM Tris pH 7.4, 0.6% Triton X-100, and protease inhibitor cocktail Halt™ Protease Inhibitor Cocktail (Thermo Fisher, PI78430). Cellular debris was removed after centrifugation at 10,000 $\times$ g for 5 min, and 20  $\mu$ g protein was used to determine A-SMase activity. A standard curve was calculated following the manufacturer's protocol and A-SMase activity initially measured in relative fluorescent units (RFU) (see Additional File 1: Fig. S1) was expressed as percentage of control.

#### Fluorescent labelling

Microglia, seeded on coverslips, were stimulated with A $\beta$ <sub>1-42</sub> peptide conjugated to Alexa 555 (AnaSpec, AS-60480-01) overnight. The next day, cells were fixed with ice-cold 4% PFA in PBS for 30 min, permeabilized with 0.25% Triton-X in PBS for 5 min and blocked with 3% BSA in PBS for 1 h. Primary antibodies, anti-Cer IgM (Glycobiotech, MAB\_0014) and anti A-SMase (Protein-Tech, 14,609-1-AP) were diluted in incubation buffer (0.3% BSA in PBS) at 4 °C overnight. Then, cells were washed 3-times with PBS and incubated with secondary antibodies for 1 h at 37 °C. Coverslips were mounted using Fluoroshield supplemented with DAPI (Sigma-Aldrich, F6057) to visualize the nuclei.

Brain tissue was processed for fluorescence labelling as previously described [25]. Briefly, after perfusion, the half-brain was fixed in 4% PFA solution and then

immersed in 30% sucrose/ PBS. Next, brains were embedded in OCT, frozen and cryosectioned at 10  $\mu$ m thickness (at  $\sim$  -20 °C; Leica). Plaques were visualized with Thioflavin S (Sigma-Aldrich, T1892) while microglia and astrocytes were immunolabeled with goat IgG anti-Iba1 (Novus Biologicals, NB100-1028) or rabbit IgG anti-gial fibrillary acidic protein (GFAP) (Wako Pure Chemical Corporation, Z0334). Astrocytic Cer was detected by co-labelling with mouse anti-GFAP antibody (Santa Cruz, sc-336773, 2E1) and rabbit anti-Cer antibody produced in our laboratory and previously validated. Secondary antibodies were Cy2-conjugated or Alexa-647 donkey anti-mouse IgG, or Cy3-conjugated donkey anti-rabbit IgG, (1:500 Jackson ImmunoResearch). Neurodegeneration was quantified with FluoroJade C (Sigma-Aldrich, AG325) staining. Images were acquired on a Nikon A1R Confocal Microscope (Nikon, New York, USA) and analyzed with Nikon NIS-Elements software or with ImageJ for microglia morphology as previously described [26]. Densitometric analysis of the stainings was performed on sagittal brain sections in hippocampus and/or cortical areas at different lateral depth (3–6 sections per animal). Identifiers for control and treatment samples were blinded to the experimenter.

#### Isolation of EVs from mouse brains

EVs were isolated from mouse forebrains as we previously described [24, 27]. In short, forebrains were digested in papain for 15 min and a 10 mL serological pipette was used to dissociate the tissue. After initial centrifugation at 300 $\times$ g for 5 min, the supernatant was subjected to centrifugation at 4000 $\times$ g (20 min), 10,000 $\times$ g (40 min) all at 4 °C and the supernatant filtered through a 0.45  $\mu$ m filter. At this point supernatants from same experimental groups were randomly paired and combined to increase EVs yield (from initial 8 forebrains of WT vehicle treated, 8 5xFAD vehicle treated and 8 5xFAD Imipramine treated we obtained N=4/group). EVs were collected using the ExoEasy Maxi kit (Qiagen, 76064) following the manufacturer's instructions.

#### Nanoparticle tracking analysis (Zetaview) and Exoview

*ZetaView*. Nanoparticle Tracking Analysis was performed using a Zetaview instrument as previously described [24]. The concentration of EVs was normalized to tissue weight of the starting material, or cell number or cellular protein when EVs were isolated from media.

*Exoview*. Equal amounts of brain- or cell culture media derived EVs were diluted in incubation buffer and loaded on pre-scanned ExoView Tetraspanin chips, placed in a sealed 24-well plate overnight at room temperature. The chips contained spots printed with anti-CD81, or anti-CD9 antibodies or mouse IgG1 $\kappa$  matching isotype

antibody, used as a control for non-specific EV binding (NanoView bioscience, EV-TETRA-MI). Chips were then moved to an automated ExoView<sup>®</sup> CW100 Chip Washer and the tetraspanin program was selected. The following antibody mixture was used to label EVs: anti-Cer IgM (Glycobiotech, MAB 0014) conjugated to Alexa 647 using a kit (Abcam, ab269823), anti-CD81 conjugated to Alexa555 (NanoView bioscience, EV-mCD81-A-555) and anti-GFAP conjugated to Alexa488 (Invitrogen, 53–9892-82), all of them diluted in blocking solution. Chips were then imaged with the ExoView R100 reader using the ExoScan 3.0 acquisition software. Images acquired were analyzed using ExoViewer 3.0 software.

### Cell death and Seahorse assay

Neuro-2a (N2a) were obtained from ATCC (CCL-131<sup>™</sup>) and maintained at 37 °C and 5% CO<sub>2</sub> atmosphere in DMEM supplemented with 10% FBS and 100U/mL penicillin–streptomycin (hyClone, GE Healthcare, UT, USA).

To determine the cytotoxicity of brain-derived EVs, N2a cells were seeded at a density of 10,000 cells/well on 96-well plates and gradually deprived of serum for 1–2 days to allow for differentiation into a neuronal phenotype and reach adequate confluency. Then, cells were treated for 18 h with 10<sup>4</sup> EVs / cell. LDH release was detected using the CyQUANT<sup>™</sup> LDH Cytotoxicity Assay (Thermo Fisher Scientific, C20300) according to the manufacturer's protocol.

N2a metabolic/bioenergetic profiles were evaluated with XF Cell Mito Stress Assay in a Seahorse XFe96/ XF96 analyzer (Seahorse Bioscience/Agilent Technologies, North Billerica, MA). N2a cells were seeded at 10<sup>4</sup> cells/well in XF microplates (Agilent, 102,416–100) and kept in 5% FBS till the next day when they were deprived of serum and challenged with 10<sup>4</sup> EVs/cell for 18 h. The media were replaced with XF assay media and a standard mito stress test assay was performed using the Seahorse flux assay. The data were normalized to cell counts using Biotek Cytation 5 (Agilent).

### Western blot

Hippocampus or astrocytes were homogenized in RIPA buffer (250 mM Tris–HCl (pH 7.4), 750 mM NaCl, 5% NP-40, 2.5% sodium deoxycholate, 0.5% SDS) with Halt<sup>™</sup> Protease Inhibitor Cocktail (Thermo Fisher, PI78430) by sonication and protein extracts were solubilized with 5X Laemmli sample buffer (10% SDS, 250 mM Tris pH 6.8, 1 mg/mL bromophenol blue, 0.5 M DTT, 50% glycerol, 5% β-mercaptoethanol) and heated to 95 °C for 5 min. Proteins were separated using SDS-PAGE gels (8 or 10%) or pre-cast gels 4–20% (mini-PROTEAN TGX, Biorad) and transferred to nitrocellulose membranes. After blocking with 5% non-fat dry milk (Blotting-grade

blocker, Biorad) for 1 h, blots were probed with primary antibodies overnight at 4 °C and incubated with HRP-conjugated secondary antibody. The membranes were developed with SuperSignal<sup>™</sup> West Pico PLUS (ThermoFisher, 34577) or SuperSignal<sup>™</sup> West Femto Substrate (ThermoFisher, 34095) and images were acquired on a ChemiDoc imaging system (Biorad). For APP and Aβ detection, membranes were probed with 1 μg / mL mAb anti-Aβ (Biolegend, 6E10, 803001). GFAP was detected with anti-GFAP from Wako Pure Chemical Corporation and C3b with ProteinTech (21337–1-AP) antibody. Bands were normalized to β-actin (Santa Cruz, sc-47778).

### Carboxylation and 3-nitrotyrosine measurements

Proteins from the cortex were extracted in Tris-buffered saline containing Halt<sup>™</sup> Protease Inhibitor Cocktail (Thermo Fisher, PI78430) by probe sonication. Detection of carbonyls and 3-nitrotyrosine was performed as previously described [28] by immunoblotting using the polyclonal antibodies RbxDNP (Oxy Blot Protein Oxidation Kit, Chemicon-Millipore, Cat No. S-150) and anti-3-NT (Thermo Fisher Scientific, RRID:AB\_221457) respectively. Membranes were scanned with a photo scanner (Epson Perfection V600), and slot-blot line densities were quantified by the ImageQuant TL software package (GE Healthcare Bio-Sciences, RRID:SCR\_014246).

### Sphingolipid analysis

The sphingolipids of astrocytes, hippocampus and brain derived EVs were quantified by the lipidomics core facility at the Medical University of South Carolina, Charleston, SC (Dr. Besim Ogretmen, director) (<https://hollingscancercenter.musc.edu/>) as previously described [29, 30]. The following sphingolipids species were determined: sphingosine, sphinganine, sphingosine-1-phosphate, sphinganine-1-phosphate, Cer (N-acyl chain lengths = C14:0, C16:0, C18:1, C18:0, C20:0, C22:0, C24:1, C24:0, C26:1, C26:0). Sphingolipid levels were normalized to protein content or number of EVs measured by NTA.

### Statistical analysis

The statistical analyses were performed using GraphPad Prism version 8.4.3 (686). Unpaired *t*-test was used for comparing of two means or Whitney Mann test when normality distribution was not met. One-way ANOVA followed by LSD or Dunnett's multiple comparisons test was used for comparing more than 2 conditions or for investigating Imipramine effect. Two-way ANOVA was used to analyze lipid measurements in the hippocampus with genotype and treatment as independent variables

followed by LSD post-doc test. A *p*-value of <0.05 was considered significant.

### Results

#### A-SMase is activated downstream of TLR4 receptor activation and translocated to the plasma membrane in response to Aβ oligomers

A-SMase is found upregulated and more active in brains of AD patients compared to controls [9]. Since it was previously reported that stimulation of immune cells activates A-SMase [31, 32], we investigated if Aβ oligomers could induce A-SMase activity in microglia. Microglia from 4 weeks old wild type (WT) mice were isolated and stimulated with 2 μM Aβ oligomers for 18 h. A-SMase was more active after stimulation with Aβ oligomers (Fig. 1A). A-SMase activation was inhibited by TLR4 receptor or A-SMase inhibitors but not by a TNF-α receptor inhibitor (Fig. 1A), which was tested to exclude TNF-α autocrine activation of A-SMase. Aβ oligomers triggered the translocation of A-SMase to the

plasma membrane and increased the co-localization of A-SMase with Cer in the plasma membrane as quantified by Pearson correlation analysis (Fig. 1B and C). Scrambled Aβ<sub>42</sub> used as a control did not induce co-localization of A-SMase with Cer in the plasma membrane, while aggregates of Aβ<sub>42</sub> led to a locally increased concentration of A-SMase and Cer (arrows in Additional File 1: Fig. S2A). Importantly, Aβ oligomer-dependent release of IL-1α, TNF-α and C1q was suppressed by ARC39 and Imipramine, a direct A-SMase inhibitor and FIASMA, respectively (Fig. 1D). This data indicates that A-SMase is activated downstream of the TLR4 receptor, and it is translocated to the plasma membrane in response to Aβ oligomers. Furthermore, A-SMase activity is critical for the secretion of IL-1α, TNF-α and C1q.

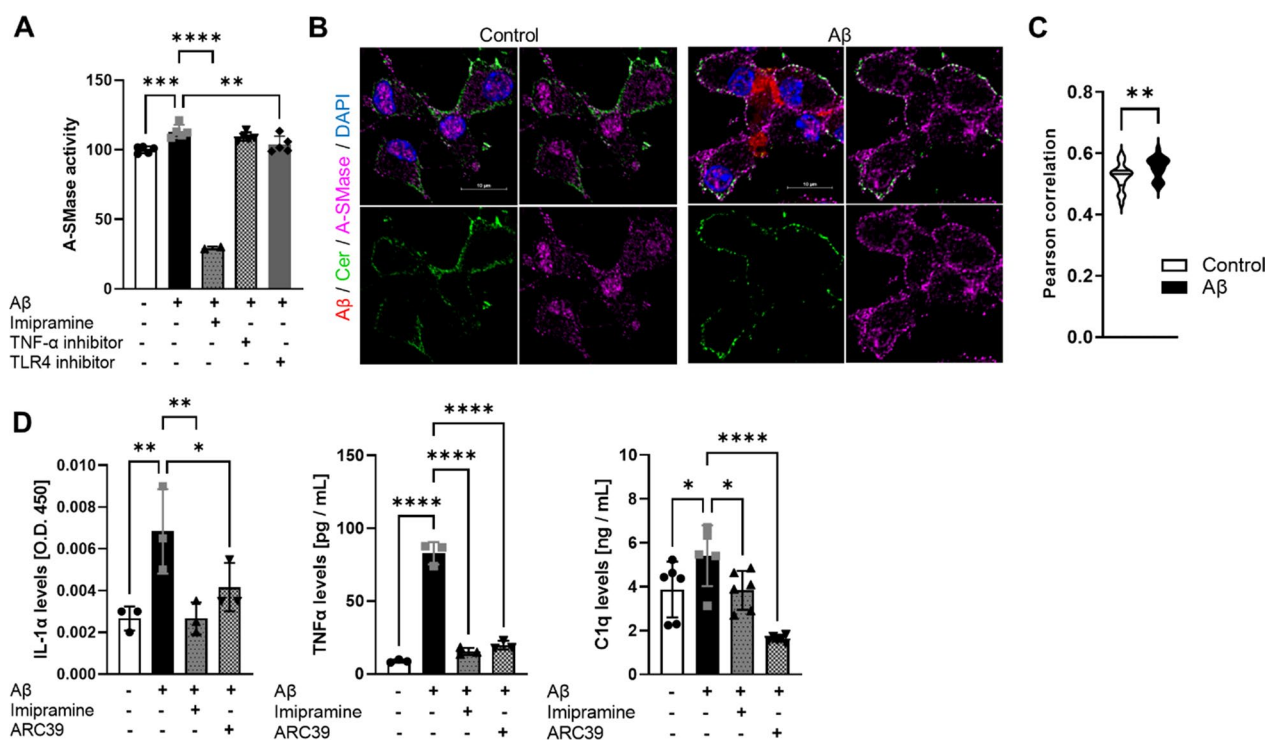


**Fig. 1** A-SMase is activated downstream of the TLR4 receptor and translocated to the plasma membrane in response to Aβ oligomers. **A** A-SMase activity expressed as percentage of control measured in microglia treated with Aβ<sub>1-42</sub> oligomers in the presence of Imipramine (10 μM) or TNFα receptor inhibitor (10 ng/mL) or TLR4 receptor inhibitor (10 μM). Bar graphs represent average ± SD of N > 3/group. One-way ANOVA, Dunnett's posthoc testing (\*\**p* < 0.01, \*\*\**p* < 0.001, \*\*\*\**p* < 0.0001). **B** Photomicrographs of primary microglia stimulated with or without Aβ<sub>1-42</sub> peptide conjugated to Alexa 555 (Red) and subsequently immunolabeled with anti-Cer (Green) and anti-A-SMase (Magenta) antibodies. Nuclei were stained with DAPI. Scale bar = 20 μm. **C** Violin plots depicting Pearson correlation coefficient between Cer and A-SMase fluorescent intensities of 4–5 photomicrographs / condition. Unpaired *t*-test (\*\**p* < 0.01). **D** IL-1α, TNFα and C1q levels measured in supernatant of primary microglia by ELISA after 18 h incubation with Aβ<sub>1-42</sub> oligomers and of 10 μM Imipramine or 5 μM ARC39. Bar graphs represent average ± SD of N > 3/group. One-way ANOVA, Dunnett's posthoc testing (\**p* < 0.05, \*\**p* < 0.01, \*\*\*\**p* < 0.0001)

**Microglia-conditioned medium increases ceramide in reactive astrocytes, which is prevented by inhibition of A-SMase**

Since inhibition of A-SMase reduced the release of pro-inflammatory factors from Aβ-treated microglia we explored whether adding A-SMase inhibitors to microglia would also prevent phenoconversion of wild type astrocytes to an active state, when incubated with medium conditioned by microglia as depicted in Fig. 2A. We did not focus on the contribution of individual factors, but tested the effect of the full range of factors added by microglia to the medium when exposed to Aβ with or without A-SMase inhibitors. As expected, astrocytes incubated with media from Aβ-treated microglia

displayed upregulation of GFAP and complement factor C3b, which was prevented when microglia were treated with A-SMase inhibitors (Fig. 2B). Previously we reported that reactive astrocytes in AD show increased levels of Cer in vivo [16, 25, 33, 34]. Therefore, we explored if media from Aβ-treated microglia would trigger astrocytic Cer formation. We found that especially C16 Cer and C24 Cer were upregulated and that treatment of microglia with A-SMase inhibitors suppressed this elevation (Fig. 2C). This data indicates that medium conditioned by Aβ-treated microglia activates astrocytes and increases astrocytic ceramide generation, which is prevented by inhibition of A-SMase.

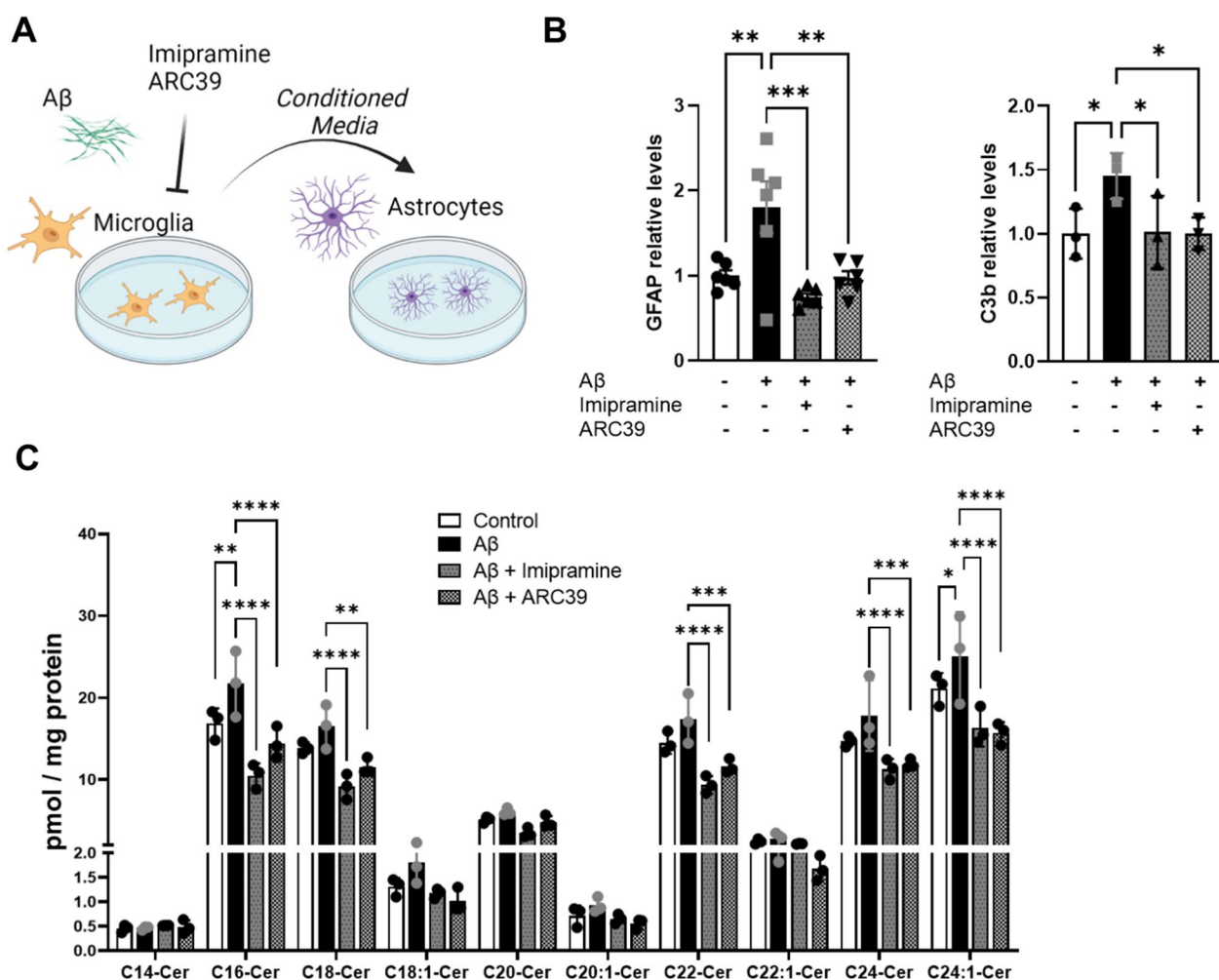


**Fig. 2** Inhibition of A-SMase prevents astrocytic Cer formation. **A** Schematic diagram showing treatment of astrocytes with microglia-conditioned media. **B** Quantification of GFAP and C3b by western blot analysis in astrocytes after 24 h incubation with conditioned media from microglia (Western blot membranes are shown in Additional File 1). Bar graphs represent average ± SD of N > 3/group. One-way ANOVA, Dunnett's posthoc testing (\*p < 0.05, \*\*p < 0.01, \*\*\*p < 0.001). **C** Quantification of C14:0, C16:0, C18:0, C18:1, C20, C20:1, C22:0, C22:1, C24:0 and C24:1 by mass spectrometry of astrocytes after incubation with conditioned media from microglia. Bar graph represents average ± SD with each N = 3 group. One-way ANOVA, Dunnett's posthoc testing (\*p < 0.05, \*\*p < 0.01, \*\*\*\*p < 0.0001)

**The proinflammatory factors IL-1 $\alpha$ , TNF- $\alpha$  and C1q trigger the release of mitotoxic Cer-enriched EVs from astrocytes**

Our data showed that conditioned medium of A $\beta$ -treated microglia contained proinflammatory cytokines, the secretion of which is prevented by the inhibition of A-SMase. It is known that (1) microglia-derived cytokines activate astrocytes [15], (2) cytokines induce secretion of EVs and ceramide generation in astrocytes, and (3) increase of ceramide levels in astrocytes is critical for the secretion of neurotoxic EVs that are enriched with ceramide [35–38]. However, we do not know if proinflammatory cytokines induce secretion of ceramide-enriched neurotoxic EVs by reactive astrocytes. Therefore, astrocytes isolated from P3 pups were stimulated for 24 h with a combination of IL-1 $\alpha$ , TNF- $\alpha$  and C1q. EVs secreted by astrocytes were isolated by ultracentrifugation as previously described [24]. Nanoparticle tracker (Zetaview) analysis showed that stimulation with proinflammatory factors increased the numbers of EVs per cell by 1.5 -fold (Fig. 3A). To test if these EVs were enriched with Cer, we used Exoview analysis, a method that immunocaptures EVs by binding to immobilized antibodies against tetraspanins (e.g., CD9) for counting of EVs and single vesicle

immunolabeling with different antibodies. The number of CD9 positive EVs was increased by 1.8-fold, consistent with the increase of total EVs as determined by Zetaview analysis (Fig. 3A and B). Immunolabeling of CD9 positive EVs was performed with a fluorophore-conjugated antibody against Cer. We found that the proportion of CD9 positive EVs immunolabeled for Cer increased by 3.3-fold in EVs from stimulated (reactive) astrocytes when compared to EVs from non-stimulated (resting) control cells (Fig. 3B). Since the number of both, total and CD9 positive EVs secreted by reactive astrocytes was increased by 1.3-fold, while the proportion of CD9 positive EVs labeled for Cer was increased by 3.3-fold, the proinflammatory factors must have induced the secretion of EVs that are enriched with Cer.

Based on previous studies showing that Cer-enriched EVs from AD brain target mitochondria [35, 39], we tested if proinflammatory factors induced secretion of mitotoxic EVs from astrocytes. Seahorse analysis showed that the Cer-enriched EVs were mitotoxic to neuronal cells (Fig. 3D and E). This data suggests that IL-1 $\alpha$ , TNF- $\alpha$  and C1q trigger the release of mitotoxic Cer-enriched EVs from astrocytes.

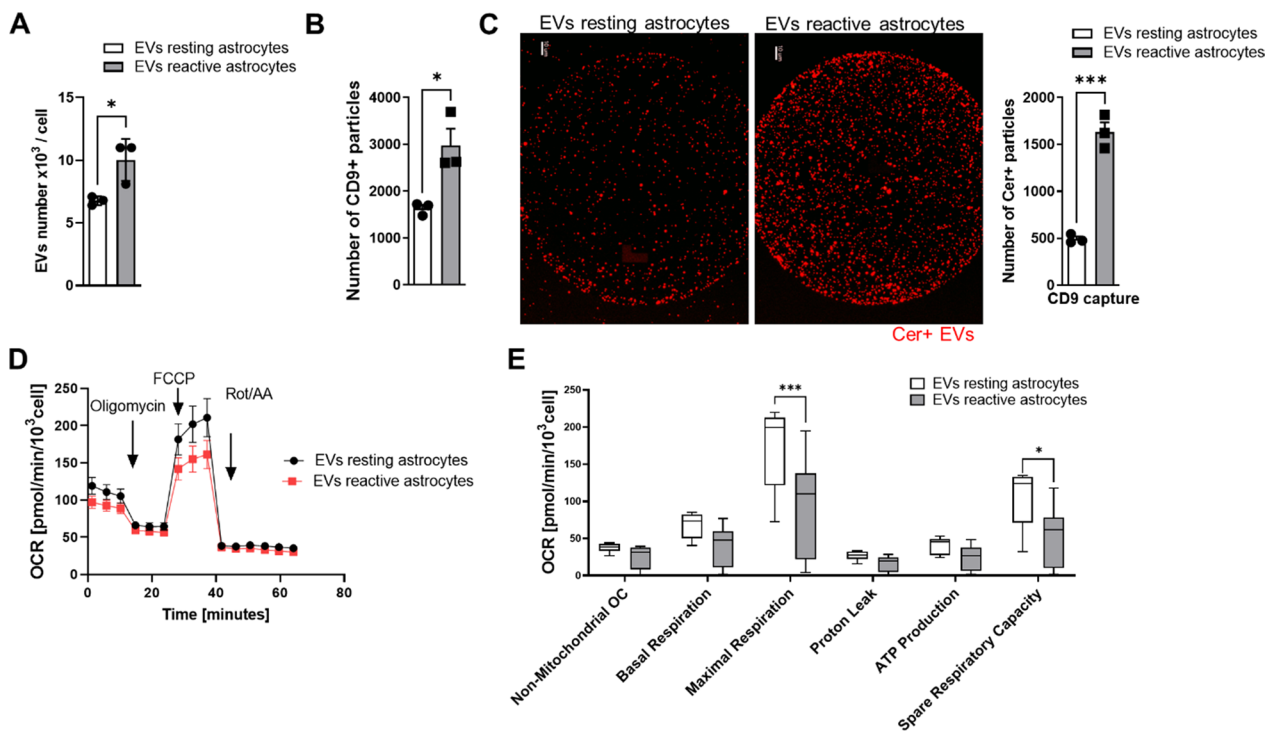


**Fig. 3** The proinflammatory factors, IL-1 $\alpha$ , TNF- $\alpha$  and C1q trigger the release of mitotoxic Cer-enriched EVs from astrocytes. **A** Numbers of EVs per cell measured by NTA after stimulation of astrocytes without (resting astrocytes) or with combination of C1q, TNF- $\alpha$  and IL-1 $\alpha$  (reactive astrocytes). Bar graphs represent N=3/group. Unpaired *t*-test (\**p* < 0.05). **B** Number of CD9-captured EVs. N=3/group. Unpaired *t*-test (\**p* < 0.05). **C** Representative images for Cer positive EVs in CD9 capture spots. Quantification of Cer + EVs. Bar graphs represent N=3/group. Unpaired *t*-test (\*\**p* < 0.001). **D** and **E** Bioenergetics of neuronal cells incubated with EVs of resting or reactive astrocytes assessed by Seahorse Flux Analyzer using Cell Mito Stress test. Lines represent average  $\pm$  SD and Whiskers plot of N=3/group. Unpaired *t*-test (\**p* < 0.05, \*\*\**p* < 0.001)

**Imipramine inhibits microglia activation and astrocytic Cer formation in vivo**

The anti-inflammatory effects of A-SMase inhibitors in vitro prompted us to investigate whether

administration of Imipramine for 4 weeks would affect glial cell activation in an AD mouse model (5xFAD mice). Iba1 is considered a constitutive marker for microglia, which is highly increased in 5xFAD animals compared

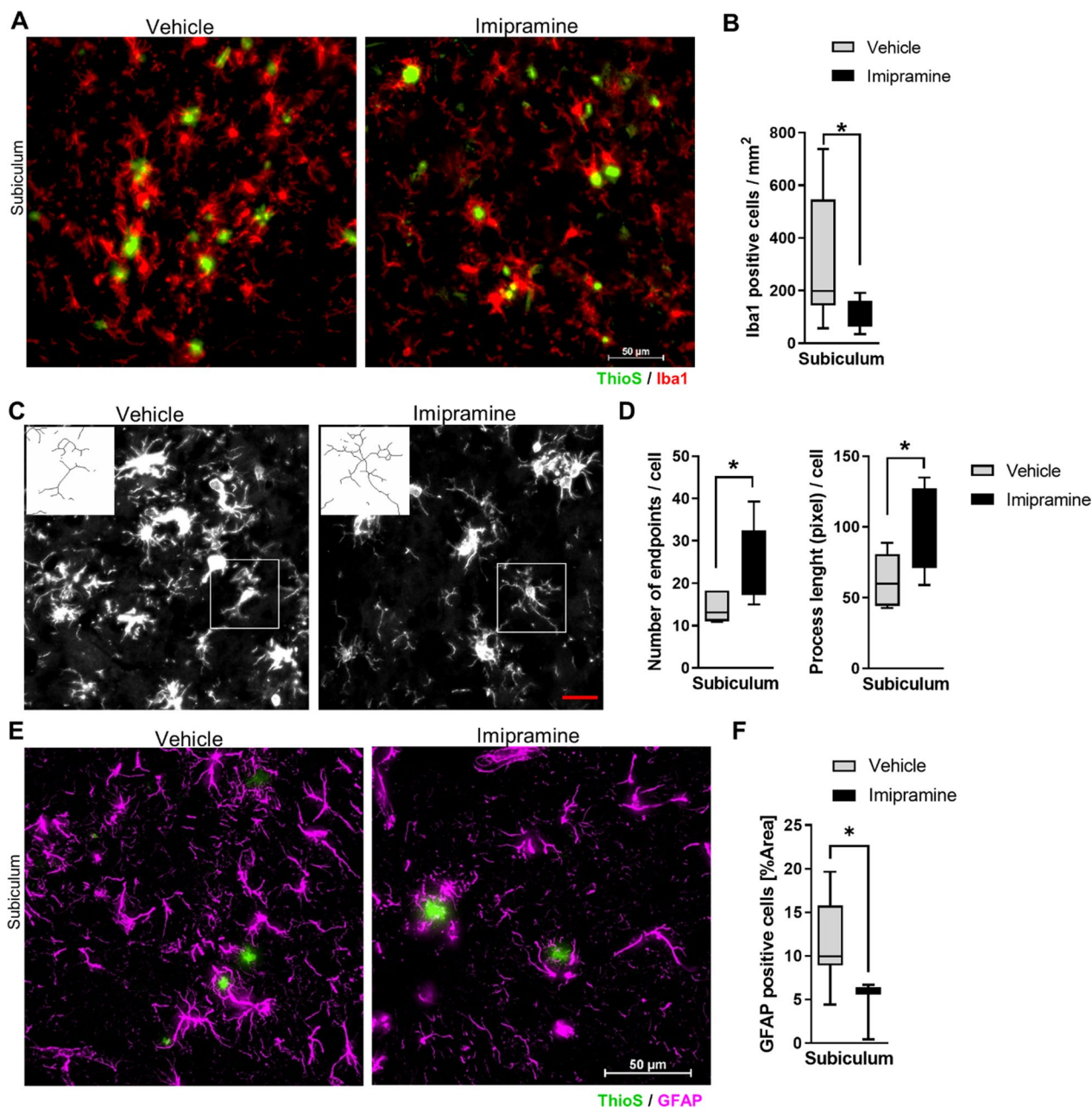


**Fig. 4** Imipramine inhibits microglia and astrocyte activation in vivo. **A** Representative photomicrograph of Iba1 staining and ThioS in the subiculum region of 5xFAD animals treated with vehicle or Imipramine (Scale bar 50  $\mu$ m). **B** Densitometric analysis of Iba1 staining represented as number of positive Iba1 cells/mm<sup>2</sup> (Vehicle N=5 and Imipramine N=5 for groups). **C** Illustrations of the microglia morphological analysis applied to a fluorescent photomicrograph captured with 40x objective with a single cell cropped to show details. Scale bar 20  $\mu$ m. **D** Number of endpoints and length of microglia ramification per cell in vehicle or Imipramine. Morphological analysis was performed on Vehicle N=5 and Imipramine N=5 for groups. **E** Representative photomicrographs of GFAP and ThioS in the subiculum region of 5xFAD animals treated with vehicle or Imipramine (Scale bar 50  $\mu$ m). **F** Box and Whiskers plot of densitometric analysis of GFAP staining represented as a percentage of the area (Vehicle N=5 and Imipramine N=5 for groups). Unpaired *t*-test (\**p*<0.05)



to WT [40, 41]. Therefore, brain sections were analyzed for Iba1 immunoreactivity. Imipramine decreased the number of Iba1 positive microglia in the subiculum (percentage of area  $p < 0.001$ ) (Fig. 4A-B). We further characterized microglia based on ramifications in the subiculum. The analysis showed that microglia in Imipramine treated 5xFAD mice had more endpoints and longer ramifications (Fig. 4C and D) suggesting an anti-inflammatory phenotype. The anti-inflammatory effect of Imipramine was confirmed by reduced labeling of microglia and astrocytes for iNOS, a marker of activated glia (Additional File 1: Fig. S3A) [42].

Next, to determine the extent of astrocytosis in the 5xFAD mouse brain treated with Imipramine compared to control, we performed GFAP immunofluorescence labeling (Fig. 4E). Densitometric analysis showed a reduced area of GFAP-labeled astrocytes in Imipramine-treated mice (Fig. 4F). When investigating the effect of Imipramine on global Cer levels in the hippocampus,

we observed that Cer d18:1/18:0 (F test interaction (1, 23)=5.087,  $p=0.0339$ ), Cer d18:1/24:0 (F test interaction (1, 21)=6.499,  $p=0.0187$ ), Cer d18:1/26:0 and Cer d18:1/26:1 (F test interaction (1, 22)=4,  $p=0.0419$ ) were elevated in 5xFAD animals compared to WT and that Imipramine reduced levels of Cer d18:1/24:0, Cer d18:1/26:0 and Cer d18:1/26:1 (Fig. 5A). Next, astrocytic Cer was assessed by immunolabeling as previously described [25]. Co-labeling of GFAP with Cer or Iba1 with Cer was significantly reduced in Imipramine-treated brains (Fig. 5B and C). This data indicates that long chain Cers are elevated early in the hippocampus of 5xFAD and that Imipramine prevents microglia and astrocyte activation and production of Cer by glial cells in vivo.

**Imipramine reduces GFAP positive and mitotoxic brain-derived EVs**

Reactive astrocytes fail to provide metabolic support to neurons, and we previously discovered that they release

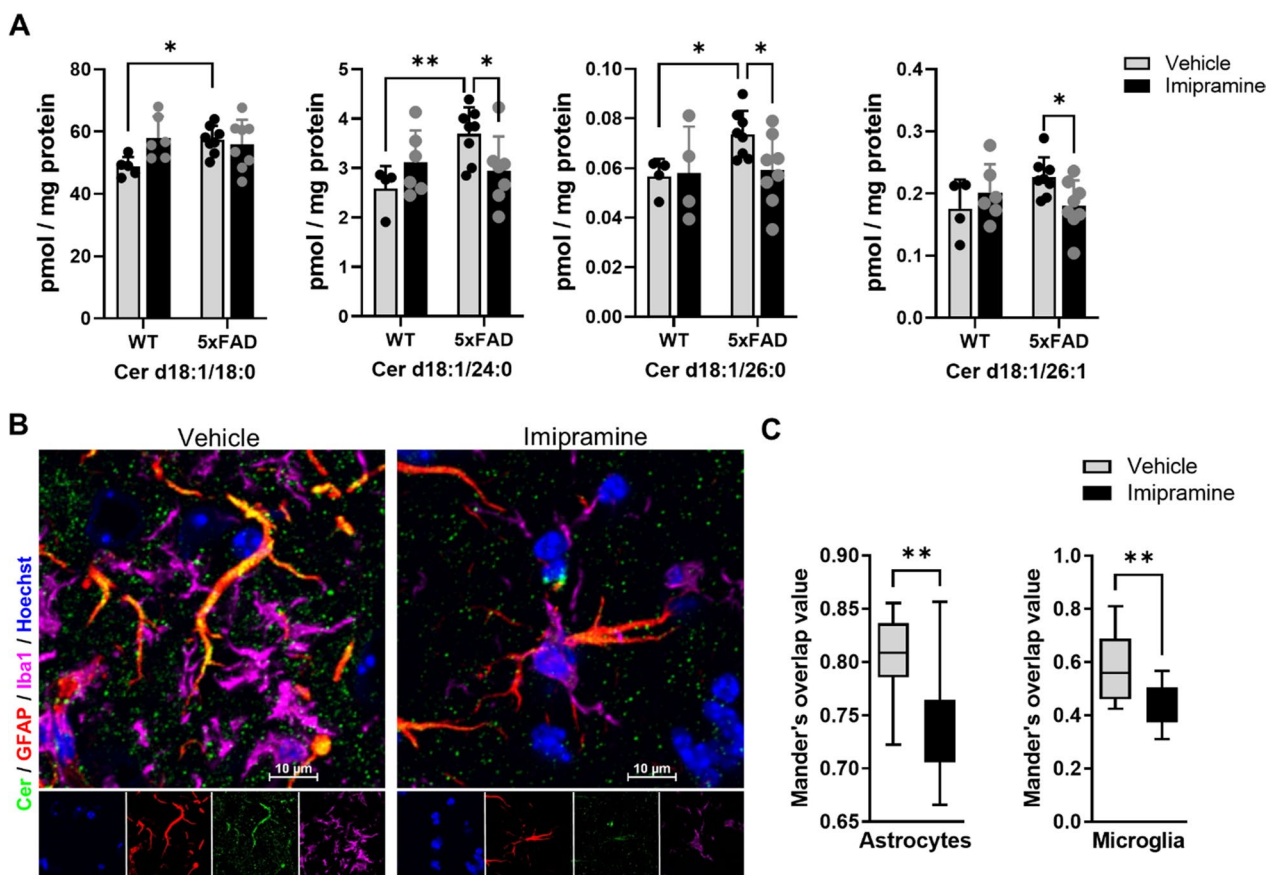


**Fig. 5** Imipramine prevents astrocytic ceramide formation in vivo. **A** E Quantification of C18:0, C24:0, C26:0 and C26:1 Cer by mass spectrometry in the hippocampus. Bar graph represents average  $\pm$  SD with each N=4–8/group. Two-way ANOVA followed by LSD postdoc analysis ( $*p < 0.05$ ,  $**p < 0.01$ ). **B** Representative photomicrographs of Iba 1 (Magenta), GFAP (Red), Cer (Green), and Hoechst (Blue) in the subiculum region of 5xFAD animals treated with vehicle or Imipramine (Scale bar 10  $\mu$ m). **C** Box and Whiskers plot of correlation analysis of GFAP and Iba1 staining with Cer immunolabelling represented as Mander's overlap values (Vehicle N=5 and Imipramine N=5 for groups). Unpaired t-test ( $**p < 0.01$ )

EVs enriched in Cer and A $\beta$  which are mitotoxic [35]. Therefore, we explored if EVs isolated from brain of Imipramine-treated mice showed reduced neurotoxicity. We found that the size and numbers of EVs extracted from the forebrain were similar between WT, 5xFAD vehicle and Imipramine-treated brains (Fig. 6A). However, the proportion of CD9 positive EVs was increased in the 5xFAD animals compared to WT. Additionally, the proportion of CD9 captured EVs, which were co-immunolabeled for GFAP and Cer was elevated in 5xFAD (Fig. 6B). Consistent with our in vitro data with reactive astrocytes (Fig. 2B and C), this data indicated that in 5xFAD mice, the proportion of astrocyte-derived, CD9 positive and Cer-enriched EVs were increased. Imipramine reduced the number of CD9 positive EVs and the number of astrocyte-derived EVs to WT levels (Fig. 6B). Furthermore, the correlation of Cer with GFAP positive EVs was reduced by 40% by Imipramine (Fig. 6C).

Consistent with a proportion of EVs enriched with Cer, mass spectrometry analysis of Cer and sphingosine species of total EVs showed that Cer d18:1/18:0 and Cer d18:1/20:0 levels were elevated in 5xFAD compared to WT, which was reduced by Imipramine (Fig. 6D). We also measured A $\beta_{1-42}$  levels in EVs and observed that Imipramine reduced A $\beta$  levels in EVs (Fig. 6E). Furthermore, when assessing the neurotoxicity of the EVs we found that Imipramine reduced their toxicity (Fig. 6F). Lastly, we measured the impact of Imipramine on the EV-induced disruption of neuronal mitochondrial function using Seahorse analysis. Consistent with our in vitro data, EVs from 5xFAD brain compromised maximal and spare respiration capacity of neuronal cells as compared to WT, which was rescued by Imipramine (Fig. 7A–C). This data indicates that Imipramine prevents astrocytic release of mitotoxic EVs by reducing the number of Cer-enriched, CD9/GFAP positive EVs and A $\beta_{1-42}$  levels in EVs.

### Imipramine prevents plaque deposition and neurodegeneration

Our data show that Imipramine decreased proinflammatory activation of microglia and astrocytes, as well as the secretion of Cer-enriched, mitotoxic EVs in 5xFAD mice. Previous studies reported that Imipramine improves

memory symptoms in AD patients [43]. Therefore, we investigated the effect of Imipramine on A $\beta$  plaque deposition and neurodegeneration. Statistical analysis showed a significant reduction in the plaque load between the 5xFAD treated with vehicle or Imipramine-treated mice, both in the cortex and subiculum (Fig. 8A and B). Additionally, the plaque size was reduced in Imipramine-treated 5xFAD brains (Fig. 8C). Furthermore, A $\beta$  quantification of brain homogenates showed that A $\beta$  levels were reduced in samples treated with Imipramine and the ratio A $\beta$ /FL-APP was decreased implying a reduction of A $\beta$  biogenesis or increased clearance of A $\beta$  (Fig. 8D). Detection of degenerating mature neurons in the subiculum by FluorJadeC confirmed a protective effect of Imipramine from AD pathology (Fig. 8E). Furthermore, 3-Nitrotyrosine levels, which are indicative of oxidative stress, were reduced in the 5xFAD drug-treated group (Fig. 8F). Importantly, no differences in the drug response were found between sexes. This data suggest that Imipramine prevents A $\beta$ -induced neurodegeneration by reducing A $\beta$  plaques and oxidative stress indicators like 3-Nitrotyrosine levels.

### Discussion

In the brain of AD patients, the enzyme A-SMase is upregulated, and the enzymatic activity abnormally high [9]. In this work, we report that A-SMase is upregulated in microglia in response to A $\beta$  oligomers via activation of the TLR4 receptor. Inhibition of A-SMase activity using Imipramine or ARC39 reduced microglia release of proinflammatory factors such as C1q, IL1- $\alpha$  and TNF- $\alpha$  which are critical for astrocyte phenocconversion to a reactive state. Additionally, Imipramine prevented increase of Cer levels in astrocytes and secretion of mitotoxic EVs.

Neuroinflammation is thought to play a crucial role in the development and exacerbation of AD pathology [44]. Genome-wide association studies implicate microglia-related pathways in AD [45]. One way in which microglia contribute to disease is by initiating an immune response when exposed to A $\beta$  oligomers, which over time becomes chronic. This causes the release of proinflammatory factors that induce astrocyte activation. Previous studies on immune cells suggested that Cer generated by A-SMase

(See figure on next page.)

**Fig. 6** Imipramine reduces ceramide, GFAP, and A $\beta$  levels in 5xFAD brain-derived EVs. **A** NTA measurement of EVs isolated from forebrain normalized to protein content of starting tissue. Bar graph represents average  $\pm$  SD with each N=4/group. **B** Representative particle counts on different CD9 capture spots. Counts of GFAP (GFAP+) and Cer (Cer+) positive EVs, CD9 captured. Bar graph represents average  $\pm$  SD. for three capture spots of N=4 (pooled)/group. **C** Representative images and pie chart showing percentage of colocalization of GFAP+ with Cer+ in CD9 captured EVs of 5xFAD vehicle and Imipramine treated groups. **D** Quantification of C14:0, C16:0, C18:0, C18:1, C20, C20:1, C22:0, C24:0, C24:1 Cer by mass spectrometry of brain EVs. Bar graph represents average  $\pm$  SD with each N=3/group. **E** A $\beta_{1-42}$  quantification in brain derived EVs by ELISA. Bar graph represents average  $\pm$  SD with each N=4/group. **F** Neuronal toxicity determined by LDH release after 18 h incubation with brain derived EVs. Box and Whiskers plot with each N=4/group. One-way ANOVA followed by Tukey postdoc (\* $p$  < 0.05, \*\* $p$  < 0.01, \*\*\* $p$  < 0.0001, \*\*\*\* $p$  < 0.0001)

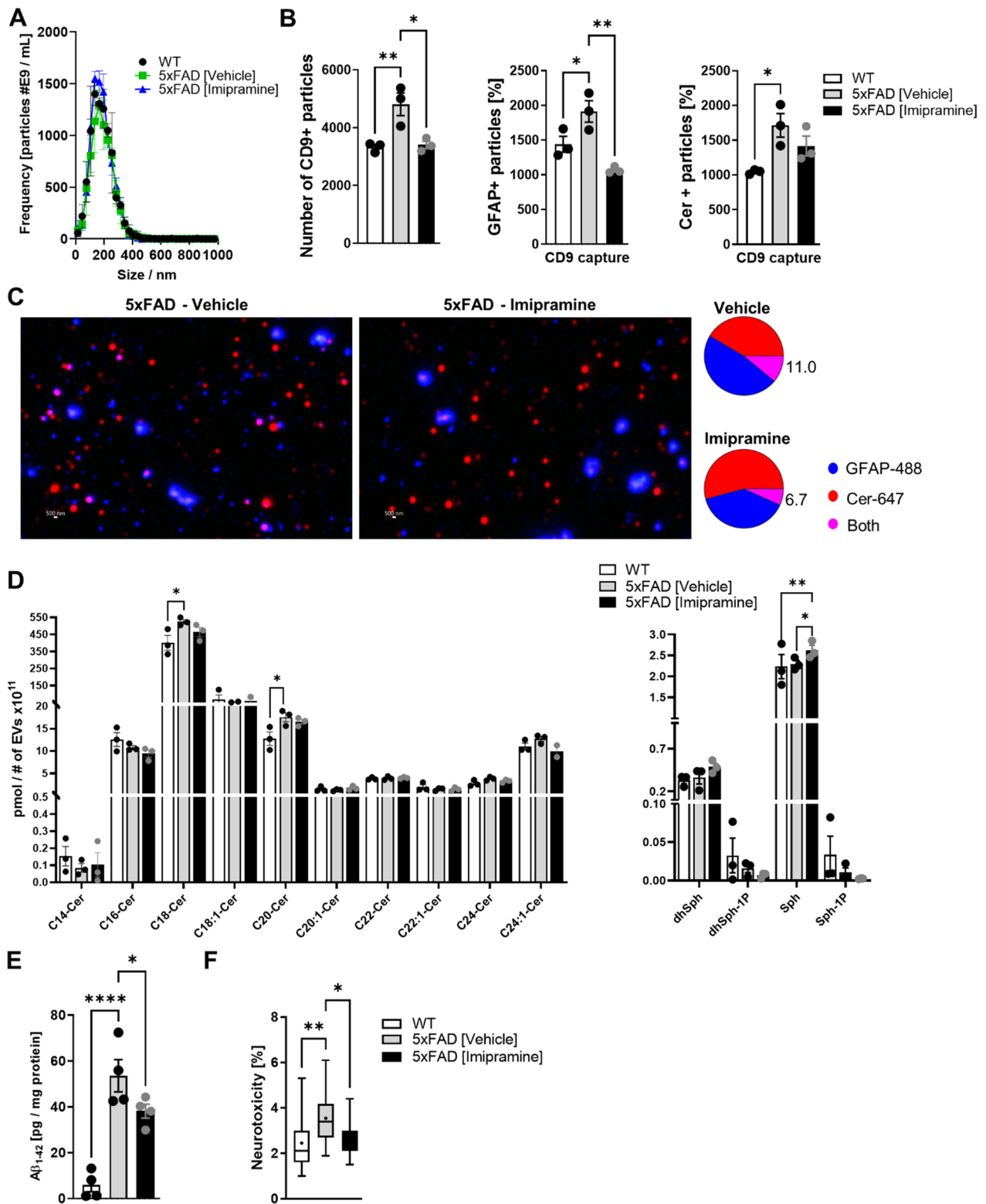


**Fig. 6** (See legend on previous page.)

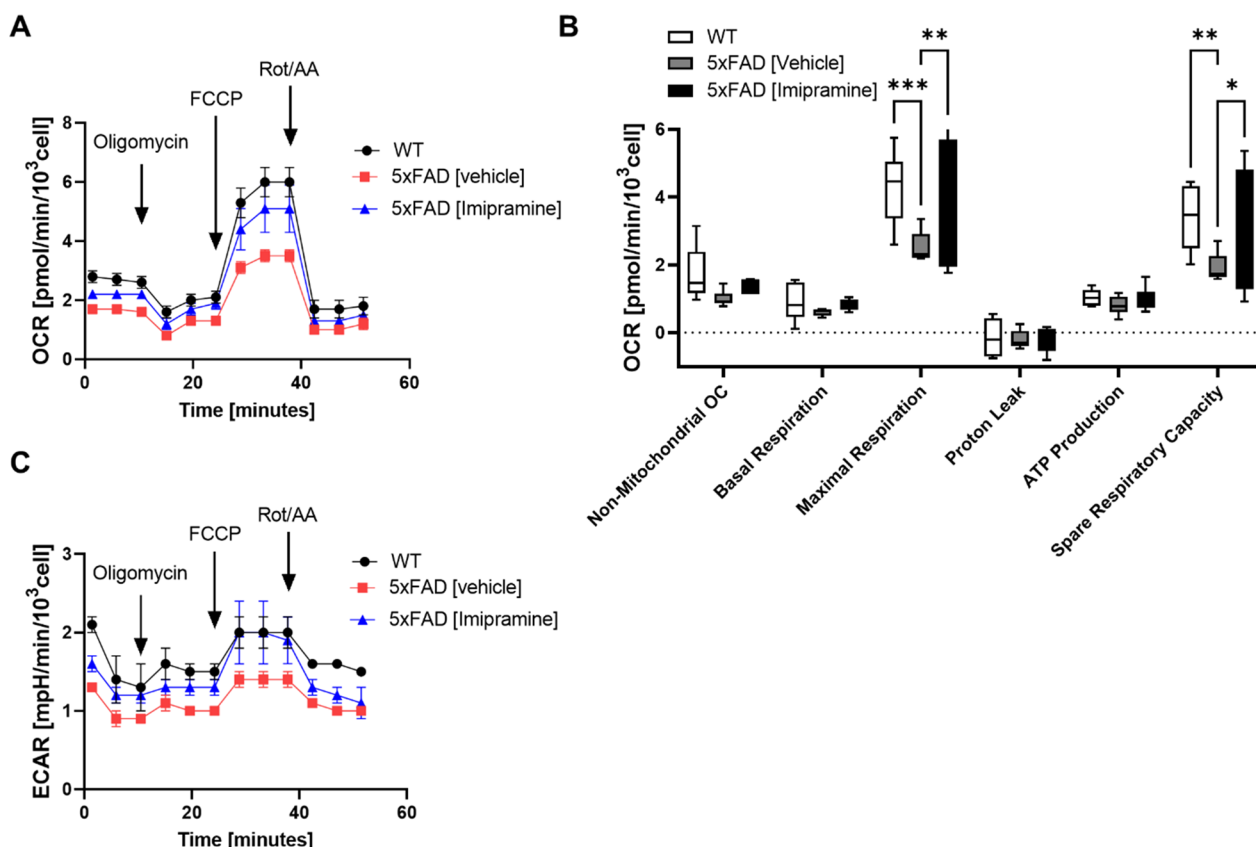


**Fig. 7** Imipramine reduces mitotoxicity of 5xFAD brain-derived EVs. **A** Bioenergetics of neuronal cells incubated with brain derived EVs of WT, 5xFAD treated with vehicle or Imipramine assessed by Seahorse Flux Analyzer using Cell Mito Stress Kit. Lines and Whiskers plot represent average  $\pm$  SD with each N = 4/group. **B** One-way ANOVA, Dunnett’s posthoc testing (\* $p$  < 0.05, \*\* $p$  < 0.01, \*\*\* $p$  < 0.001). **C** Extracellular acidification rate (ECAR) of neuronal cells incubated with brain-derived EVs of WT, 5xFAD mice treated with vehicle or Imipramine. Lines represent average  $\pm$  SD with each N = 4/group

is critical for cytokine release [31, 32]. It was also reported that activation of the TLR4 receptor requires Cer generation by A-SMase in immune cells [46]. Additionally, immunohistochemistry analysis in the brain of AD patients suggested that A-SMase was mostly associated with microglia [34]. However, others have shown that A-SMase activity is elevated in neuronal cells and fibroblasts isolated from AD transgenic models [11]. We found that A-SMase activity in microglia was increased by A $\beta$  oligomers and required TLR4 receptor activation. We excluded that activation was due to TNF- $\alpha$  auto-crine action by including an TNF- $\alpha$  inhibitor in the assay. Our experiment did not exclude the possibility of direct action of A $\beta$  oligomers on A-SMase activity. As previously reported A-SMase was required for the secretion of proinflammatory factors like C1q, IL1- $\alpha$  and TNF- $\alpha$  [31, 32]. Also, in vivo inhibition of A-SMase with Imipramine reduced the number of activated microglia suggesting that the A-SMase/Cer pathway in microglia is a target for reducing neuroinflammation.

We previously discovered that reactive astrocytes are characterized by the elevation of Cer levels in the brain of AD patients and mice models of AD [16, 25, 34]. Once in the reactive state, astrocytes release a population of EVs that target neurons compromising mitochondria function [35]. These EVs are characterized by enrichment in Cer and A $\beta$ . The high concentration of Cer in these EVs increases dramatically the mitotoxic effect of A $\beta$  [35]. In addition, we reported that the enzyme neutral sphingomyelinase 2 (N-SMase2) played a critical role in generating these toxic EVs [47]. When inactivating N-SMase2 genetically or pharmacologically, brain EVs were lower in number and characterized by reduced levels of Cer and A $\beta$  [47]. These findings encouraged the synthesis of additional N-SMase2 inhibitors as potential therapeutics for AD [48]. However, targeting N-SMase2 seemed to be ineffective in female 5xFAD mice, suggesting that other enzymes of the sphingolipid pathway are involved in forming these toxic EVs. While evidence of sexual dimorphism is gaining more attention in EVs research,

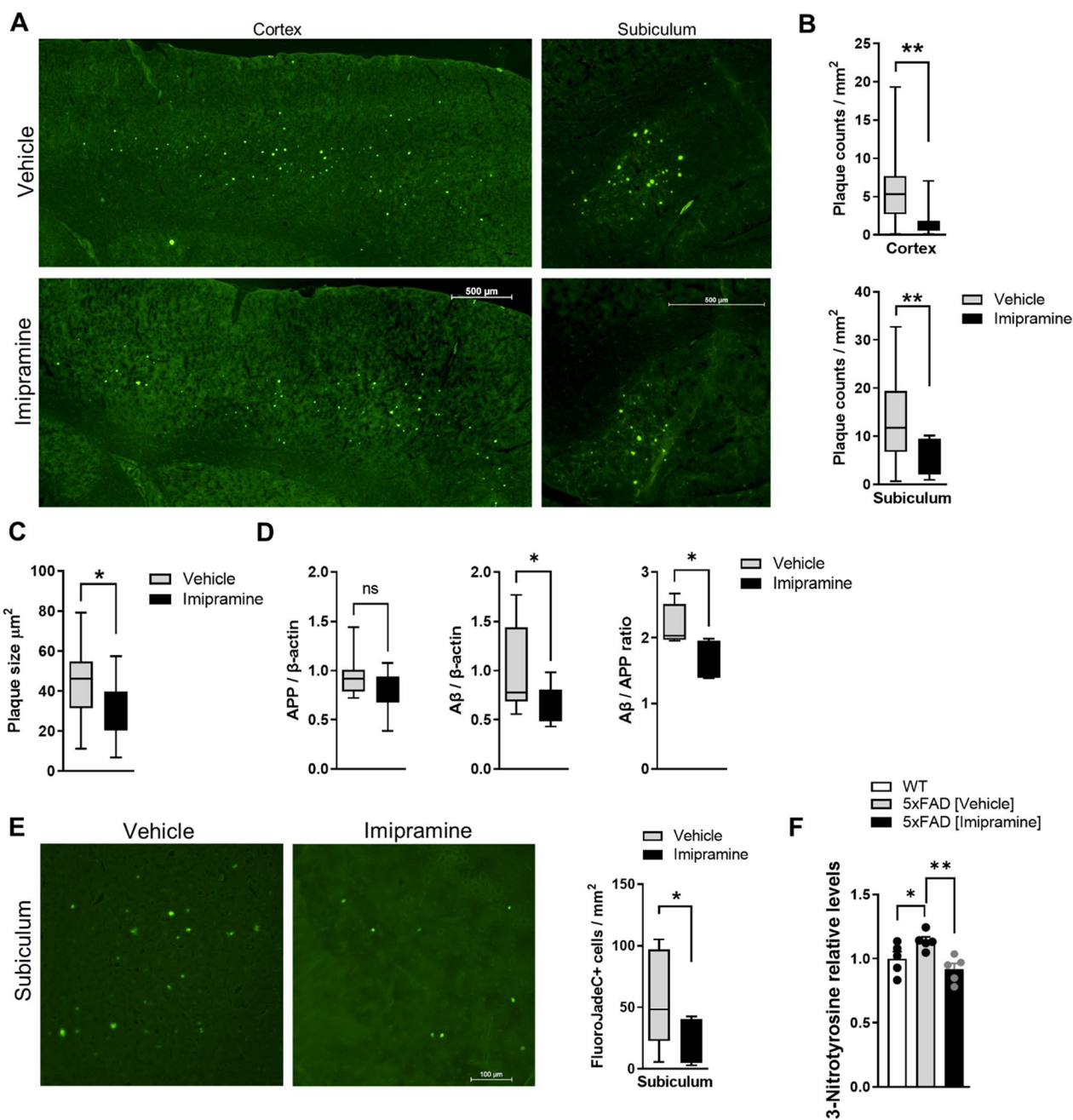


**Fig. 8** Imipramine prevents plaques deposition and neuronal cell death. **A** Representative photomicrographs of sagittal brain sections imaging the cortex and subiculum of 5xFAD labeled Aβ plaques in green. All photomicrographs were exposed and processed identically. Scale bar represents 500 μm. **B** Immunofluorescence quantification of plaques measured by plaques counts/mm<sup>2</sup> and in **C** Plaques size area. **D** Western blot analysis of hippocampal homogenate stained with 6E10 antibody showing APP and Aβ levels normalized to β-actin and the ratio of amyloid Aβ/APP. Western blot membranes are shown in Additional File 1. **E** Representative photomicrographs and quantification of FluoroJadeC positive cells (Green staining) in the subiculum. Box and Whiskers plot of 4–5 animals per experimental condition, Unpaired *t*-test was applied (*\*p* < 0.05, *\*\*p* < 0.01). **F** Quantification of 3-Nitrotyrosine relative levels in pre-frontal cortex of WT, 5xFAD vehicle and Imipramine groups. Bar graphs represent the mean ± SD of N = 5/group. One-way ANOVA, LSD (*\*p* < 0.05, *\*\*p* < 0.01)

it is poorly studied in AD. We recently found that A-SMase is associated with brain derived EVs and it is highly expressed in 5xFAD, especially female 5xFAD [27].

Concomitantly to the increase of A-SMase expression, brain-derived-EVs of female 5xFAD are characterized by

the elevation of long chain Cer [27], clearly showing that A-SMase plays a critical role in Cer enrichment of EVs.

In the current study, we found that Imipramine reduced the number of EVs derived from astrocytes and diminished the content of A $\beta$  in EVs while only modestly lowering the Cer concentration in the total population of EVs. However, Imipramine depleted Cer associated to EVs derived from astrocytes by 40%. Inhibition of A-SMase was sufficient to drastically reduce the mitotoxicity of 5xFAD brain derived EVs. Notably, EVs derived from the brain of 5xFAD show upregulation of Cer 18:1/18:0 and Cer 18:1/20:0 and mitotoxicity already at 3 months of age, before any memory deficits are detectable by behavioral paradigms.

It is important to highlight that the beneficial effect of Imipramine may arise from targeting A-SMase in several cell types and cell signaling pathways. In microglia, our data show that A-SMase is critical for the A $\beta$ -induced secretion of proinflammatory factors through the TLR4-pathway. In astrocytes, A-SMase controls the release of large size vesicles after stimulation of ATP receptors [49]. Bianco et al., reported that activation of A-SMase was downstream to p38 MAPK cascade, which is also activated in response to TLR4 ligands [50]. In addition, they showed that the p38 MAPK cascade mobilizes A-SMase from the lysosome to the plasma membrane triggering membrane blebbing and EVs formation. While Bianco et al. did not show that cytokines induce secretion of EV or characterizes the lipid profile of these EVs, they found that A-SMase is released with these population of EVs. Other studies showed that cytokines such as Il-1 $\beta$  or TNF- $\alpha$  can induce EV secretion by astrocytes, however, these studies did not investigate the function of A-SMase or enrichment of EVs with ceramide [36, 37].

In our work, we found that CD9 positive EVs derived from astrocytes were mostly affected by proinflammatory factors and Imipramine treatment. The factors C1q, IL1- $\alpha$  and TNF- $\alpha$  triggered the secretion of a 1.8-fold increase of CD9 positive EVs from astrocytes and A-SMase inhibition reduced CD9 positive EVs and Cer levels associated with astrocytic EVs. Interestingly, CD9 positive EVs were associated with EV generated by blebbing of the plasma membrane [51]. Therefore, Cer generated by A-SMase in the plasma membrane or endolysosomal membranes in reactive astrocytes could be critical for the formation of toxic EVs. This mechanism is supported by our recent study showing that fluoxetine, another FIASMA similar to Imipramine, prevents complex formation between ceramide-enriched cellular membranes in astrocytes and A $\beta$  [52]. While this mechanism is consistent with our data, it is also clear that neither A-SMase nor the effect of A-SMase inhibition is confined to a particular cell type. Hence, alternative mechanisms to be tested could include

the effect of microglia-derived EVs on astrocytes or astrocytic EVs on or microglia. Therefore, in future studies we will further investigate the A-SMase/Cer pathway in reactive astrocytes and its critical function for toxic EV generation.

Tricyclic anti-depressants (TCAs), such as Imipramine, have been used in the treatment of the depressive symptoms in AD. Depression is one of the common comorbidities of AD that appears during the progression of the disease [53]. Treatment of AD with antidepressants has been successful not only in controlling depressive symptoms but also in rescuing the cognitive decline [43]. Moreover, anti-depressants given to AD animal models demonstrated to be effective in coping with depressive as well as cognitive symptoms [54–56]. While TCAs are known to block serotonin and norepinephrine transporters, recent studies suggest that their activity as FIASMAs reducing forebrain ceramide levels critically contributes to their anti-depressant effect [57–59]. Therefore, it is reasonable to imply the reduction of ceramide as a potential mechanism by which Imipramine contributes to mitigation of AD pathology.

In line with this proposed mechanism, partial ablation of A-SMase expression in the AD mice model reduced A $\beta$  pathology and prevented memory impairment [11]. More recently, new approaches using different ASM inhibitors or immunotherapy with antibodies against A-SMase were shown to alleviate AD pathology, however, these studies did not address the function of A-SMase in glial activation and the secretion of neurotoxic EVs [60, 61]. FIASMAs such as Imipramine reduce Cer levels, glial activation, and the secretion of neurotoxic EVs in the brain, and they are clinically approved and immediately available for AD therapy.

In this study, we found that Imipramine prevented plaque formation in the cortex and subiculum. Furthermore, neuronal death was strongly diminished in the Imipramine-treated group. Nevertheless, the choice of FIASMA that are also tricyclic anti-depressants will need to be carefully tested. For example, long term administration of anti-depressants like escitalopram, showed to be inefficient in controlling plaques disease and even contraindicated [62]. Therefore, the synthesis or discovery of specific A-SMase blockers, will help to answer whether in vivo inhibition of A-SMase during AD pathology is an effective therapy [63].

## Conclusion

In conclusion, we report that A-SMase is activated in microglia by A $\beta$  oligomers via TLR4 receptor. The Cer generated by A-SMase is critical for the release of C1q, TNF- $\alpha$  and IL1- $\alpha$ , which induce the reactive astrocytes phenotype. Administration of Imipramine to 5xFAD for 4

weeks prevented microglia and astrocyte activation. Furthermore, brain derived-EVs from 5xFAD mice treated with Imipramine were less mitotoxic and displayed reduction in astrocytic marker GFAP and A $\beta$  concentration when compared to EVs derived from 5xFAD brain treated with vehicle. Our study highlights A-SMase as a target in AD to prevent microglia and astrocytes activation, and warrants synthesis and testing of brain permeable compounds, which specifically inhibit A-SMase as anti-AD therapeutic strategy.

#### Abbreviation

AD	Alzheimer's disease
A-SMase	Acid sphingomyelinase
EVs	Extracellular vesicles
Cer	Ceramide
A $\beta$	Amyloid- $\beta$
TCA	Tricyclic anti-depressant
FIASMA	Functional inhibitors of A-SMase
WT	C57BL/6 wild type
IP	Intraperitoneally
PFA	Paraformaldehyde
C1q	Complement component 1
IL-1 $\alpha$	Interleukin 1 $\alpha$
TNF $\alpha$	Tumor necrosis factor $\alpha$
GFAP	Glial fibrillary acidic protein
CD9	Cluster of differentiation 9

#### Supplementary Information

The online version contains supplementary material available at <https://doi.org/10.1186/s40478-023-01633-7>.

**Additional file 1. Supplementary Fig. 1:** A Standard curve built with known pmol of A-SMase and measured relative fluorescent units (RFU). **B** Representative experiment showing A-SMase activity expressed in RFU of 20  $\mu$ g of microglia lysate stimulated with A $\beta$  oligos in presence of Imipramine and TNF- $\alpha$  inhibitor. **Supplementary Fig. 2:** Primary cultures of microglia were incubated with 1  $\mu$ M scrambled A $\beta$ 42 or A $\beta$ 42 overnight. Immunocytochemistry was performed with antibodies against A $\beta$ 42 (4G8), A-SMase (Proteintech rabbit IgG), and ceramide (mouse IgM, Glycobiotech MAB0014). **Supplementary Fig. 3:** Cryosections (cortex) were immunolabeled for A $\beta$ 42 (rabbit IgG, ThermoFisher), iNOS (mouse IgG, BDBiosciences), and Iba-1 (goat IgG, Novus). **Immunoblot images. A** Immunoblots showing detection of GFAP and **B** C3b protein expression. **C**  $\beta$ -actin was used as internal control. **D** Immunoblots showing detection of FL-APP, and A $\beta$  bands with 6E10 antibody. **E**  $\beta$ -actin was used as internal control.

#### Acknowledgements

Acknowledgement is made to the donors of ADR, a program of BrightFocus Foundation, for support of this research. Additionally, we would like to acknowledge the Markey Shared Resource Facility which is supported by the NCI Cancer Center Support Grant (P30 CA177558). In addition, we acknowledge the support of the Department of Physiology (Chair Dr. Alan Daugherty) at the University of Kentucky College of Medicine.

#### Author contributions

EB and SMC conceived the project and designed the experiments. SMC and EB performed the microscope experiments. SMC, AE and ZQ performed EV isolation and characterization. ZZ, SMC and PT performed Western blotting and other immunoassays. SMC and LZ contributed to the production of primary neurons and the in vivo experiments. SMC and EB contributed to the analysis and interpretation of lipid measurements. SMC and EB wrote the

manuscript. HJV and PGS performed, analyzed and interpreted the Seahorse measurements. All authors contributed by critically revising the manuscript.

#### Funding

This work was supported by grants to EB (National Institutes of Health: R01AG064234, R21AG078601, RF1AG078338; U.S. Department of Veterans Affairs: I01BX003643) and to SMC (BrightFocus Grant Submission No.: A20201464F; National Institute On Aging of the National Institutes of Health under Award Number P30AG028383). PGS and HV received support from Kentucky Spinal Cord and Head Injury Research Trust (KSCHIRT chair #3).

#### Availability of data and materials

The datasets used and/or analyzed during the current study are available from the corresponding author on reasonable request.

#### Declarations

##### Ethics approval and consent to participate

All experiments using mice to generate primary cell cultures or drug testing were carried out according to an Animal Use Protocol approved by the Institutional Animal Care and Use Committee at the University of Kentucky (Protocol No. 2017–2677).

##### Consent for publication

Not applicable.

##### Competing interests

The authors declare that they have no competing interests.

Received: 15 June 2023 Accepted: 5 August 2023

Published online: 21 August 2023

#### References

- Couttas TA et al (2018) Age-dependent changes to sphingolipid balance in the human hippocampus are gender-specific and may sensitize to neurodegeneration. *J Alzheimers Dis* 63:503–514. <https://doi.org/10.3233/JAD-171054>
- Cutler RG et al (2004) Involvement of oxidative stress-induced abnormalities in ceramide and cholesterol metabolism in brain aging and Alzheimer's disease. *Proceed Nat Acad Sci USA* 101:2070–2075. <https://doi.org/10.1073/pnas.0305799101>
- Han X, McKeel DMH, Kelley DW, Kelley J, Morris JC (2002) Substantial sulfatide deficiency and ceramide elevation in very early Alzheimer's disease: potential role in disease pathogenesis. *J Neurochem* 82(809):818
- Filippov V et al (2012) Increased ceramide in brains with Alzheimer's and other neurodegenerative diseases. *J Alzheimers Dis* 29:537–547. <https://doi.org/10.3233/JAD-2011-111202>
- Mielke MM et al (2010) Serum sphingomyelins and ceramides are early predictors of memory impairment. *Neurobiol Aging* 31:17–24. <https://doi.org/10.1016/j.neurobiolaging.2008.03.011>
- Mielke MM et al (2012) Serum ceramides increase the risk of Alzheimer disease: the Women's Health and Aging Study II. *Neurology* 79:633–641. <https://doi.org/10.1212/WNL.0b013e318264e380>
- Fonteh AN et al (2015) Sphingolipid metabolism correlates with cerebrospinal fluid Beta amyloid levels in Alzheimer's disease. *PLoS One* 10:e0125597. <https://doi.org/10.1371/journal.pone.0125597>
- Katsel P, Li C, Haroutunian V (2007) Gene expression alterations in the sphingolipid metabolism pathways during progression of dementia and Alzheimer's disease: a shift toward ceramide accumulation at the earliest recognizable stages of Alzheimer's disease? *Neurochem Res* 32:845–856. <https://doi.org/10.1007/s11064-007-9297-x>
- He X, Huang Y, Li B, Gong CX, Schuchman EH (2010) Deregulation of sphingolipid metabolism in Alzheimer's disease. *Neurobiol Aging* 31:398–408. <https://doi.org/10.1016/j.neurobiolaging.2008.05.010>
- Crivelli SM et al (2020) Sphingolipids in Alzheimer's disease, how can we target them? *Adv Drug Deliv Rev*. <https://doi.org/10.1016/j.addr.2019.12.003>

11. Lee JK et al (2014) Acid sphingomyelinase modulates the autophagic process by controlling lysosomal biogenesis in Alzheimer's disease. *J Exp Med* 211:1551–1570. <https://doi.org/10.1084/jem.20132451>
12. Li X, Gulbins E, Zhang Y (2012) Oxidative stress triggers Ca-dependent lysosome trafficking and activation of acid sphingomyelinase. *Cell Physiol Biochem* 30:815–826. <https://doi.org/10.1159/000341460>
13. Wiegmann K, Schutze S, Machleidt T, Witte D, Kronke M (1994) Functional dichotomy of neutral and acidic sphingomyelinases in tumor necrosis factor signaling. *Cell* 78:1005–1015. [https://doi.org/10.1016/0092-8674\(94\)90275-5](https://doi.org/10.1016/0092-8674(94)90275-5)
14. Butterfield DA, Lauderback CM (2002) Lipid peroxidation and protein oxidation in Alzheimer's disease brain: potential causes and consequences involving amyloid beta-peptide-associated free radical oxidative stress. *Free Radic Biol Med* 32:1050–1060. [https://doi.org/10.1016/s0891-5849\(02\)00794-3](https://doi.org/10.1016/s0891-5849(02)00794-3)
15. Liddelow SA et al (2017) Neurotoxic reactive astrocytes are induced by activated microglia. *Nature* 541:481–487. <https://doi.org/10.1038/nature21029>
16. Wang G et al (2012) Astrocytes secrete exosomes enriched with proapoptotic ceramide and prostate apoptosis response 4 (PAR-4): potential mechanism of apoptosis induction in Alzheimer disease (AD). *J Biol Chem* 287:21384–21395. <https://doi.org/10.1074/jbc.M112.340513>
17. Dinkins MB, Dasgupta S, Wang G, Zhu G (2014) & Bieberich, E 2014 Exosome reduction in vivo is associated with lower amyloid plaque load in the 5XFAD mouse model of Alzheimer's disease. *Neurobiol Aging*. <https://doi.org/10.1016/j.neurobiolaging.2014.02.012>
18. Kim MH et al (2017) Hepatic inflammatory cytokine production can be regulated by modulating sphingomyelinase and ceramide synthase 6. *Int J Mol Med* 39:453–462. <https://doi.org/10.3892/ijmm.2016.2835>
19. Albouz S et al (1981) Tricyclic antidepressants induce sphingomyelinase deficiency in fibroblast and neuroblastoma cell cultures. *Biomedicine* 35:218–220
20. Yoshida Y et al (1985) Reduction of acid sphingomyelinase activity in human fibroblasts induced by AY-9944 and other cationic amphiphilic drugs. *J Biochem* 98:1669–1679
21. Kolzer M, Werth N, Sandhoff K (2004) Interactions of acid sphingomyelinase and lipid bilayers in the presence of the tricyclic antidepressant desipramine. *FEBS Lett* 559:96–98. [https://doi.org/10.1016/S0014-5793\(04\)00033-X](https://doi.org/10.1016/S0014-5793(04)00033-X)
22. Hurwitz R, Ferlinz K, Sandhoff K (1994) The tricyclic antidepressant desipramine causes proteolytic degradation of lysosomal sphingomyelinase in human fibroblasts. *Biol Chem Hoppe Seyler* 375:447–450
23. Kornhuber J et al (2010) 2010 Functional Inhibitors of Acid Sphingomyelinase (FIASMAS): a novel pharmacological group of drugs with broad clinical applications. *Cell Physiol Biochem* 26:9–20. <https://doi.org/10.1159/000315101>
24. Crivelli SM et al (2022) Function of ceramide transfer protein for biogenesis and sphingolipid composition of extracellular vesicles. *J Extracell Vesicles* 11:e12233. <https://doi.org/10.1002/jev2.12233>
25. Crivelli SM et al (2020) Ceramide analog [18F]F-HPA-12 detects sphingolipid imbalance in the brain of Alzheimer's disease transgenic mice by functioning as a metabolic probe. *Scient Reports* 10:19354. <https://doi.org/10.1038/s41598-020-76335-4>
26. Crivelli SM et al (2021) CERTL reduces C16 ceramide, amyloid-beta levels, and inflammation in a model of Alzheimer's disease. *Alzheimers Res Ther* 13:45. <https://doi.org/10.1186/s13195-021-00780-0>
27. Elsherbini A et al (2023) Novel isolation method reveals sex-specific composition and neurotoxicity of small extracellular vesicles in a mouse model of Alzheimer's disease. *Cells* 12(12):1623. <https://doi.org/10.3390/cells12121623>
28. Hubbard WB, Harwood CL, Geisler JG, Vekaria HJ, Sullivan PG (2018) Mitochondrial uncoupling prodrug improves tissue sparing, cognitive outcome, and mitochondrial bioenergetics after traumatic brain injury in male mice. *J Neurosci Res* 96:1677–1688. <https://doi.org/10.1002/jnr.24271>
29. Bielawski J et al (2010) Sphingolipid analysis by high performance liquid chromatography-tandem mass spectrometry (HPLC-MS/MS). *Adv Exp Med Biol* 688:46–59. [https://doi.org/10.1007/978-1-4419-6741-1\\_3](https://doi.org/10.1007/978-1-4419-6741-1_3)
30. Bielawski J et al (2009) Comprehensive quantitative analysis of bioactive sphingolipids by high-performance liquid chromatography-tandem mass spectrometry. *Methods Mol Biol* 579:443–467. [https://doi.org/10.1007/978-1-60761-322-0\\_22](https://doi.org/10.1007/978-1-60761-322-0_22)
31. Sakata A et al (2007) Acid sphingomyelinase inhibition suppresses lipopolysaccharide-mediated release of inflammatory cytokines from macrophages and protects against disease pathology in dextran sulphate sodium-induced colitis in mice. *Immunology* 122:54–64. <https://doi.org/10.1111/j.1365-2567.2007.02612.x>
32. Bai A, Guo Y (2017) Acid sphingomyelinase mediates human CD4(+) T-cell signaling: potential roles in T-cell responses and diseases. *Cell Death Dis* 8:e2963. <https://doi.org/10.1038/cddis.2017.3603>
33. Zhu Z et al (2022) Neutral sphingomyelinase 2 mediates oxidative stress effects on astrocyte senescence and synaptic plasticity transcripts. *Mol Neurobiol* 59:3233–3253. <https://doi.org/10.1007/s12035-022-02747-0>
34. de Wit NM et al (2019) Astrocytic ceramide as possible indicator of neuroinflammation. *J Neuroinflammation* 16:48. <https://doi.org/10.1186/s12974-019-1436-1>
35. Elsherbini A et al (2020) Association of Abeta with ceramide-enriched astrosomes mediates Abeta neurotoxicity. *Acta Neuropathol Commun* 8:60. <https://doi.org/10.1186/s40478-020-00931-8>
36. Chaudhuri AD et al (2018) TNFalpha and IL-1beta modify the miRNA cargo of astrocyte shed extracellular vesicles to regulate neurotrophic signaling in neurons. *Cell Death Dis* 9:363. <https://doi.org/10.1038/s41419-018-0369-4>
37. Wang K et al (2017) TNF-alpha promotes extracellular vesicle release in mouse astrocytes through glutaminase. *J Neuroinflammation* 14:87. <https://doi.org/10.1186/s12974-017-0853-2>
38. Willis CM, Sutter P, Rouillard M, Crocker SJ (2020) The effects of IL-1beta on astrocytes are conveyed by extracellular vesicles and influenced by Age. *Neurochem Res* 45:694–707. <https://doi.org/10.1007/s11064-019-02937-8>
39. Elsherbini A, Bieberich E (2018) Ceramide and exosomes: a novel target in cancer biology and therapy. *Adv Cancer Res* 140:121–154. <https://doi.org/10.1016/bs.acr.2018.05.004>
40. Girard SD et al (2014) Onset of hippocampus-dependent memory impairments in 5XFAD transgenic mouse model of Alzheimer's disease. *Hippocampus* 24:762–772. <https://doi.org/10.1002/hipo.22267>
41. Savage JC et al (2015) Nuclear receptors license phagocytosis by trem2+ myeloid cells in mouse models of Alzheimer's disease. *J Neurosci* 35:6532–6543. <https://doi.org/10.1523/JNEUROSCI.4586-14.2015>
42. Asimwe N, Yeo SG, Kim MS, Jung J, Jeong NY (2015) Nitric oxide: exploring the contextual link with Alzheimer's disease. *Oxid Med Cell Longev* 2016:7205747. <https://doi.org/10.1155/2016/7205747>
43. Mokhber N et al (2014) Comparison of sertraline, venlafaxine and desipramine effects on depression, cognition and the daily living activities in Alzheimer patients. *Pharmacopsychiatry* 47:131–140. <https://doi.org/10.1055/s-0034-1377041>
44. Heppner FL, Ransohoff RM, Becher B (2015) Immune attack: the role of inflammation in Alzheimer disease. *Nature reviews. Neuroscience* 16:358–372. <https://doi.org/10.1038/nrn38803>
45. Efthymiou AG, Goate AM (2017) Late onset Alzheimer's disease genetics implicates microglial pathways in disease risk. *Mol Neurodegener* 12:43. <https://doi.org/10.1186/s13024-017-0184-x>
46. Cuschieri J, Bulger E, Billgrin J, Garcia I, Maier RV (2007) Acid sphingomyelinase is required for lipid Raft TLR4 complex formation. *Surg Infect (Larchmt)* 8:91–106. <https://doi.org/10.1089/sur.2006.050>
47. Dinkins MB et al (2016) Neutral sphingomyelinase-2 deficiency ameliorates Alzheimer's disease pathology and improves cognition in the 5XFAD mouse. *J Neurosci* 36:8653–8667. <https://doi.org/10.1523/JNEUROSCI.1429-16.2016>
48. Sala M et al (2020) Novel Human Neutral Sphingomyelinase 2 Inhibitors as Potential Therapeutics for Alzheimer's Disease. *J Med Chem* 63:6028–6056. <https://doi.org/10.1021/acs.jmedchem.0c00278>
49. Bianco F et al (2009) Acid sphingomyelinase activity triggers microparticle release from glial cells. *EMBO J* 28:1043–1054. <https://doi.org/10.1038/emboj.2009.45>
50. Zbinden-Foncea H, Deldicque L, Pierre N, Francaux M, Raymackers JM (2012) TLR2 and TLR4 activation induces p38 MAPK-dependent phosphorylation of S6 kinase 1 in C2C12 myotubes. *Cell Biol Int* 36:1107–1113. <https://doi.org/10.1042/CBI20120081>
51. Mathieu M et al (2021) Specificities of exosome versus small ectosome secretion revealed by live intracellular tracking of CD63 and CD9. *Nat Commun* 12:4389. <https://doi.org/10.1038/s41467-021-24384-2>



52. Zhu Z et al (2023) The S1P receptor 1 antagonist Ponesimod reduces TLR4-induced neuroinflammation and increases Aβ clearance in 5XFAD mice. *EBioMedicine* 94:104713. <https://doi.org/10.1016/j.ebiom.2023.104713>
53. Berger AK, Fratiglioni L, Winblad B, Backman L (2005) Alzheimer's disease and depression: preclinical comorbidity effects on cognitive functioning. *Cortex* 41:603–612
54. Wang DD et al (2016) Desipramine improves depression-like behavior and working memory by up-regulating p-CREB in Alzheimer's disease associated mice. *J Integr Neurosci* 15:247–260. <https://doi.org/10.1142/S021963521650014X>
55. Cirrito JR et al (2011) Serotonin signaling is associated with lower amyloid-beta levels and plaques in transgenic mice and humans. *Proceed Natl Acad Sci USA* 108:14968–14973. <https://doi.org/10.1073/pnas.1107411108>
56. Nelson RL et al (2007) Prophylactic treatment with paroxetine ameliorates behavioral deficits and retards the development of amyloid and tau pathologies in 3xTgAD mice. *Exp Neurol* 205:166–176. <https://doi.org/10.1016/j.expneurol.2007.01.037>
57. Kornhuber J et al (2011) Identification of novel functional inhibitors of acid sphingomyelinase. *PLoS One* 6:e23852. <https://doi.org/10.1371/journal.pone.0023852>
58. Gulbins E et al (2015) A central role for the acid sphingomyelinase/ceramide system in neurogenesis and major depression. *J Neurochem* 134:183–192. <https://doi.org/10.1111/jnc.13145>
59. Kornhuber J, Muller CP, Becker KA, Reichel M, Gulbins E (2014) The ceramide system as a novel antidepressant target. *Trends Pharmacol Sci* 35:293–304. <https://doi.org/10.1016/j.tips.2014.04.003>
60. Choi BJ et al (2023) Immunotherapy targeting plasma ASM is protective in a mouse model of Alzheimer's disease. *Nat Commun* 14:1631. <https://doi.org/10.1038/s41467-023-37316-z>
61. Park MH et al (2022) Discovery of a dual-action small molecule that improves neuropathological features of Alzheimer's disease mice. *Proc Natl Acad Sci USA*. <https://doi.org/10.1073/pnas.2115082119>
62. von Linstow CU et al (2017) Serotonin augmentation therapy by escitalopram has minimal effects on amyloid-beta levels in early-stage Alzheimer's-like disease in mice. *Alzheimers Res Ther* 9:74. <https://doi.org/10.1186/s13195-017-0298-y>
63. Arenz C (2010) Small molecule inhibitors of acid sphingomyelinase. *Cell Physiol Biochem* 26:1–8. <https://doi.org/10.1159/000315100>

## Publisher's Note

Springer Nature remains neutral with regard to jurisdictional claims in published maps and institutional affiliations.

Ready to submit your research? Choose BMC and benefit from:

- fast, convenient online submission
- thorough peer review by experienced researchers in your field
- rapid publication on acceptance
- support for research data, including large and complex data types
- gold Open Access which fosters wider collaboration and increased citations
- maximum visibility for your research: over 100M website views per year

At BMC, research is always in progress.

Learn more [biomedcentral.com/submissions](https://biomedcentral.com/submissions)

